

# When does vapor pressure deficit drive or reduce evapotranspiration?

**A. Massmann<sup>1</sup>, P. Gentine<sup>1</sup>, C. Lin<sup>2</sup>**

<sup>4</sup><sup>1</sup>Department of Earth and Environmental Engineering, Columbia University, New York, NY 10027

<sup>5</sup><sup>2</sup>Department of Hydraulic Engineering, Tsinghua University, Beijing, CN

## **Key Points:**

- <sup>7</sup> • = enter point 1 here =
- <sup>8</sup> • = enter point 2 here =
- <sup>9</sup> • = enter point 3 here =

10      **Abstract**

11      = enter abstract here =

12      **1 Introduction**

13      Changes to vapor pressure deficit (VPD) alter the atmospheric demand for water from  
 14      the land surface. Traditionally, atmospheric scientists and hydrometeorologists generally  
 15      think that an increase in atmospheric demand induces an increases in evapotranspiration  
 16      (ET) (citations?). This possible misconception developed in part due to the proliferation of  
 17      studies examining potential ET rather than estimates of ET itself (citations?). In contrast, plant  
 18      physiologists know that stomata have evolved to optimally regulate the exchange of water  
 19      and carbon, and tend to close in response to increased atmospheric dryness [Ball *et al.*, 1987;  
 20      Leuning, 1990; MEDLYN *et al.*, 2011]. Therefore, an increase (decrease) in VPD may not  
 21      correspond to an increase (decrease) in ET because stomatal closure (opening) can cancel the  
 22      effects of shifts to atmospheric demand.

← This section  
needs to be  
fleshed out,  
and I defi-  
nitely need  
to add more  
citations

23      Quantifying the plant response to a perturbation to atmospheric VPD increases our un-  
 24      derstanding of land surface response to shifts in atmospheric conditions. If plant response  
 25      reduces ET in response to atmospheric drying then soil moisture will be conserved. An in-  
 26      crease in ET in response to atmospheric drying will reduce soil moisture, but contribute in-  
 27      creased moistening to the atmosphere. Clearly, the sign and magnitude of land-surface  
 28      response drives the co-evolution of the atmosphere and land-surface at many timescales, from  
 29      diurnal to interdecadal.

30      In order to quantify plant response to perturbations to atmospheric demand for water,  
 31      we apply a Penman-Monteith framework to eddy-covariance observation spanning various  
 32      biomes and climates. Section 2 describes the data used, Section 3 derives the framework,  
 33      Section 4 presents results, and Section 5 discusses conclusions. The goal of this paper is  
 34      to use reasonable approximations as a tool to increase intuition for plant response to atmo-  
 35      spheric drying. This intuition will aid interpretation of observations and full complexity cli-  
 36      mate models.

37      **2 Methods**

38      The Penman-Monteith equation (hereafter PM) estimates ET as a function of atmo-  
 39      spheric and land-surface variables:

40

$$ET = \frac{\Delta R + g_a \rho_a c_p D_s}{\Delta + \gamma(1 + \frac{g_a}{g_s})}, \quad (1)$$

41 where variable definitions are given in Table 1. *MEDLYN et al.* [2011] developed a  
 42 model for  $g_s$  by combining optimal photosynthesis theory with empirical approaches. The  
 43 result for leaf-scale stomatal resistance was:

44

$$g_{l-s} = g_0 + 1.6 \left( 1 + \frac{g_1}{\sqrt{D_s}} \right) \frac{A}{c_s} \quad (2)$$

45 This can be adapted to an ecosystem-scale stomatal resistance by multiplying by leaf  
 46 area index (LAI) and converting units to  $\text{m s}^{-1}$

47

$$g_s = \text{LAI} \frac{RT}{P} \left( g_0 + 1.6 \left( 1 + \frac{g_1}{\sqrt{D_s}} \right) \frac{A}{c_s} \right) \quad (3)$$

48 While Equation 3 can be used in PM, it will make analytical work with the function  
 49 intractable because  $A$  is a function of ET itself. To remove dependence of ET on  $A$  we can  
 50 use the semi-empirical results of *Zhou et al.* [2015]. *Zhou et al.* [2015] showed that:

51

$$uWUE = \frac{GPP \cdot \sqrt{D}}{ET} \quad (4)$$

52 is relatively constant across time and space (within plant functional type). If, following *Lin*  
 53 *et al.* [2015], we approximate  $g_0$  as 0, we can use uWUE to remove  $A$  from  $g_s$  in a way that  
 54 makes PM analytically tractable:

55

$$g_s = \frac{RT}{P} 1.6 \left( 1 + \frac{g_1}{\sqrt{D_s}} \right) \frac{\sigma uWUE ET}{c_s \sqrt{D}} \quad (5)$$

56 Note that  $uWUE$  is fit on the ecosystem scale in *Zhou et al.* [2015] so GPP in 4 is re-  
 57 ally  $A \cdot \text{LAI}$ . This leads to the cancelation of LAI in additoin to uWUE in Equation 2. We  
 58 also recognize that our use of  $uWUE$  introudes considerable uncertainty, so we added an  
 59 uncertainty parameter  $\sigma = f(t, \text{site})$  modifying  $uWUE$ . The meaning of this parameter will  
 60 be elaborated on after the derivation of  $\frac{\partial ET}{\partial D}$ .

61 Next, plugging Equation 5 into Equation 1 and rearranging gives:

$$62 \quad ET = \frac{\Delta R + \frac{g_a P}{T} \left( \frac{c_p D_s}{R_{air}} - \frac{\gamma c_s \sqrt{D}}{1.6 R * \sigma uWUE (1 + \frac{g_1}{\sqrt{D}})} \right)}{\Delta + \gamma} \quad (6)$$

63 We can then take the derivative with respect to  $D$  to analytically determine ecosystem  
 64 response to atmospheric demand perturbations:

$$65 \quad \frac{\partial ET}{\partial D} = \frac{g_a P}{T(\Delta + \gamma)} \left( \frac{c_p}{R_{air}} - \frac{\gamma c_s}{1.6 R * \sigma uWUE} \left( \frac{2g_1 + \sqrt{D}}{2(g_1 + \sqrt{D})^2} \right) \right) \quad (7)$$

66 The  $D$  dependence in Equation 7 is a little opaque. However, mean  $D$  is 1062 Pa, so  
 67  $\sqrt{D}$  is  $32.6 \text{ Pa}^{1/2}$ , which is much less than  $g_1$  (with the exception of ENF; Table 3). So a se-  
 68 ries expansion in the limit  $\frac{\sqrt{D}}{g_1} \rightarrow 0$  gives an approximation which makes the functional form  
 69 more clear:

$$70 \quad \frac{\partial ET}{\partial D} \approx \frac{g_a P}{T(\Delta + \gamma)} \left( \frac{c_p}{R_{air}} - \frac{\gamma c_s}{1.6 R * \sigma uWUE} \left( \frac{1}{g_1} - \frac{3\sqrt{D}}{2g_1^2} + \frac{2\sqrt{D}^2}{g_1^3} - \frac{5\sqrt{D}^3}{2g_1^4} + O\left(\left(\frac{\sqrt{D}}{g_1}\right)^4\right) \right) \right) \quad (8)$$

71 Note that given yearly  $uWUE$  from Zhou *et al.* [2015],  $g_1$  from Lin *et al.* [2015] [as  
 72 presented in Franks *et al.*, 2017], and observations of  $R$ ,  $T$ ,  $P$ ,  $D_s$ , and wind speed (WS), all  
 73 quantities in Equations 7 and 8 are known except for the uncertainty parameter  $\sigma$ . With flux  
 74 tower observations of ET,  $\sigma$  will then be uniquely determined for each observation through  
 75 Equation 6:

$$76 \quad \sigma = -\frac{g_a \gamma c_s \sqrt{D_s} P}{(ET(\Delta + \gamma) - \Delta R - g_a \rho_a c_p D_s) 1.6 R T uWUE (1 + \frac{g_1}{\sqrt{D_s}})} \quad (9)$$

77 This  $\sigma$  will be some part uncertainty associated with assumptions about constant  $g_1$   
 78 and  $uWUE$ , including differences between the data used here and in the fits in Zhou *et al.*  
 79 [2015] and Lin *et al.* [2015], but also some part general PM model and FLUXNET observa-  
 80 tional uncertainty. By calculating a unique  $\sigma$  for each observation we will propagate any  
 81 model and observational uncertainty forward into our expression for  $\frac{\partial ET}{\partial D}$ .

**Table 1.** Definition of symbols and variables

Variable	Description	Units
$e_s$	saturation vapor pressure	Pa
$T$	temperature	K
$\Delta$	$\frac{\partial e_s}{\partial T}$	Pa K <sup>-1</sup>
$R$	net radiation at land surface minus ground heat flux	W m <sup>-2</sup>
$g_a$	atmospheric conductance	m s <sup>-1</sup>
$\rho_a$	air density	kg m <sup>-3</sup>
$c_p$	specific heat capacity of air at constant pressure	J K <sup>-1</sup> kg <sup>-1</sup>
$D$	VPD	Pa
$\gamma$	psychrometric constant	Pa K <sup>-1</sup>
$g_s$	stomatal conductance	m s <sup>-1</sup>
$g_{l-s}$	leaf-scale stomatal conductance	mol m <sup>-2</sup> s <sup>-1</sup>
$R^*$	universal gas constant	J mol <sup>-1</sup> K <sup>-1</sup>
$LAI$	leaf area index	-
$\sigma$	ratio of LAI to $LAI_{ref}$ in Zhou <i>et al.</i> [2015]	-
$c_s$	CO <sub>2</sub> concentration	$\mu$ mol CO <sub>2</sub> mol <sup>-1</sup> air

<sup>a</sup>Footnote text here.

87   **Table 2.** Plant functional types, their abbreviation, Medlyn coefficient [from *Lin et al.*, 2015], and uWfUE  
 88   [from *Zhou et al.*, 2015]. Note that units are converted such that the quantities fit into Equations 1-8 with the  
 89   variables in Table 1.

Abbreviation	PFT	$g_1$ ( $\text{Pa}^{0.5}$ )	uWUE ( $\mu\text{-mol [C]} \text{ Pa}^{0.5} \text{ J}^{-1} [\text{ET}]$ )
CRO	cropland	183.1	3.80
CSH	closed shrub	148.6	2.18
DBF	deciduous broadleaf forest	140.7	3.12
ENF	evergreen needleleaf forest	74.3	3.30
GRA	grassland (C3)	166.0	2.68

“Footnote text here.

### 83   **3 Data**

84   We use data from FLUXNET2015. Because  $g_1$  coefficients [*Lin et al.*, 2015] and uWUE  
 85   were only both available for five plant functional types (PFTs - see Table 3), only 56 of the 77  
 86   sites were used. Figure 1 presents each site and its plant functional type.

← map needs  
to be im-  
proved - it's  
a placeholder  
for now

92   We restrict our analysis to the daytime (sensible heat  $> 5 \text{ W m}^{-2}$  and shortwave radia-  
 93   tion  $> 50 \text{ W m}^{-2}$ ) when there is no precipitation and the plants are growing (GPP  $> 10\%$  of  
 94   the 95th percentile). Also, because some sites use half hourly data but some use hourly, we  
 95   aggregate all data to hourly averages. Only times with good quality control flags are used.

← This GPP  
thresholding  
was used by  
Changjie, do  
you know if  
there is a ci-  
tation for it?  
Otherwise it  
seems like  
something  
a reviewer  
would have  
issue with as  
it is arbitray

### 96   **4 Results**

97   By construction, the variability in the  $\sigma$  term (Equation 9) contains all model and ob-  
 98   servational uncertainties. For an observation that perfectly matches our model and assump-  
 99   tions  $\sigma$  will be one. Therefore, if for our assumptions and framework to be reasonable  $\sigma$   
 100   should be  $O(1)$ . Figure 2 presents the histogram of calculated  $\sigma$ s with outliers (lowest and  
 101   highest 5% percent) and nonphysical values ( $\sigma < 0$ ) removed. All remaining  $\sigma$  values are  
 102    $O(1)$  which provides confidence in model framework.

106   An additional concern is that the  $\sigma$  term may in fact be some function of  $D$ , in which  
 107   case the dependence would need to be accounted for when taking the derivative. Figure 3  
 108   plots the joint distribution of  $\sigma$  and VPD, and shows that  $\sigma$  is very weakly a function of

← Figs 2 and 3  
can probably  
be combined  
- the his-  
togram of  $\sigma$   
is shown in  
Fig 3.

109 VPD. Given this weak dependence, we argue that Equation 7 is a valid approximation for  
 110 ET response to  $D$ .

115 Before calculating the sensitivity of ET to VPD, it is useful to consider the functional  
 116 form of Equation 7. There are three terms: a scaling term for the full expression we will call  
 117 Term 1 ( $\frac{g_a P}{T(\Delta+\gamma)}$ ), a relatively constant offset we will call Term 2 ( $\frac{c_p}{R_{air}}$ ), and a variable term  
 118 we will call Term 3 ( $\frac{\gamma c_s}{1.6 R \text{ uWUE}} \left( \frac{2g_1 + \sqrt{D}}{2(g_1 + \sqrt{D})^2} \right)$ ). All variables are positive, so the relative mag-  
 119 nitude between Term 2 and Term 3 will determine the sign of the derivative, while Term 1  
 120 will scale the expression larger or smaller.

121 In Term 1,  $\frac{P}{T} \propto \rho$ , so this should vary little relative to  $g_a$  and  $\Delta$ .  $\gamma$  should also be rel-  
 122 atively constant. So the scaling term, Term 1, should be primarily a function of  $g_a$  and tem-  
 123 perature (through the function  $\Delta$ ). While temperature range may vary for PFT, the functional  
 124 form of  $\Delta$  will be the same.  $g_a$  will vary strongly with PFT due to the importance of surface  
 125 roughness. However, the coefficient of variability for both  $g_a$  and Term 1 is relatively con-  
 126 stant across PFT, suggesting that the influence of  $g_a$  on the relative (to the mean) variability  
 127 of Term 1 is approximately similar across PFT.

128 Figure 4A shows Term 1 normalized by mean  $g_a$  (calculated for each plant functional  
 129 type), and confirms that much of the relative variability of Term 1 is contained in the  $g_a$   
 130 term's relative variability. Generally,  $T$  has less of a role. Additionally, the impact of  $T$  on  
 131 the relative variability increases with increasing  $g_a$ .

132 While the relative variability of Term 1 is similar across PFT, the absolute value of  
 133 Term 1 varies strongly across PFT. Figure 4B shows Term 1 evaluated with the mean  $g_a$  for  
 134 each PFT, and at the range of observed temperatures for each PFT. As expected, for the tree  
 135 PFTs (DBF, ENF) Term 1 is much larger and the temperature dependence is much stronger.  
 136 Systematic differences in observed temperatures also cause differences in the average mag-  
 137 nitude of Term 1. For example, ENF experiences on average colder temperatures and is thus  
 138 more likely to have a larger scaling term. Additionally, because  $\text{std}(g_a) \propto \overline{g_a}$ , the spread of  
 139 Term 1 due to  $g_a$  variability will be larger for the tree PFTs, although this is not shown for  
 140 simplicity. To summarize, the variability of Term 1 within each PFT will look like Figure 4A  
 141 for each PFT, but the scale of the x and y-axis will increase or decrease according to mean  $g_a$   
 142 observed in Figure 4B.

147 Term 2 minus Term 3 determines the sign of the sensitivity of ET to VPD and is thus  
 148 crucial.  $c_s$  variability is relatively less than  $\sigma$  and  $D$  variability, then variability within PFT  
 149 will be solely determined by  $\sigma$  and  $D$  at the different fluxnet sites. Figure 5 shows how (Term  
 150 2 - Term 3) varies with  $D$  and  $\sigma$ , as a function of PFT. In Figure 5a lower uWUE and  $\sigma$   
 151 shift the distribution of (Term 2 - Term 3) towards negative values. Additionally, the smaller  
 152  $g_1$ , the greater the relative  $D$  dependence of (Term 2 - Term 3). This is observed most  
 153 strongly for the ENF PFT, which has the smallest  $g_1$  (74.31).

160 Figure 5b shows the location of the minima of ET, as a function of  $\sigma$  and  $D$ . For any  $\sigma$   
 161 or VPD less (more) than these curves, Term 2 - Term 3 will be negative (positive). It is clear  
 162 that the portion of VPD observations below/above these curves will be a strong function of  
 163  $\sigma$ . However, we can see some general trends. For CSH,  $\frac{\partial ET}{\partial D}$  should be negative for the vast  
 164 majority of observed  $\sigma$  and VPD. The fraction of positive  $\frac{\partial ET}{\partial D}$  appears to be more even for  
 165 ENF, GRA, and DBF, and we might expect a greater frequency of positive  $\frac{\partial ET}{\partial D}$  for CRO.

166 Table 3 confirms these expectations for PFT behavior of  $\frac{\partial ET}{\partial D}$ . For all PFTs except for  
 167 CRO, average  $\frac{\partial ET}{\partial D}$  is less than zero. However,  $\frac{\partial ET}{\partial D}$  evaluated at the average of all variables  
 168 (e.g.  $\sigma$ ,  $T$ ,  $c_s$ ,  $D$ ) is only negative for CSH and GRA. And, DBF in addition to CRO experiences  
 169  $\frac{\partial ET}{\partial D} < 0$  less than half the time. These observations highlight the effect of the nonlin-  
 170 ear function in Figure 5:  $\frac{\partial ET}{\partial D}$  has a much steeper slope when the function is negative, and is  
 171 thus more likely to be large.

172 The units of  $\frac{\partial ET}{\partial D}$  make it difficult to interpret if  $D$  is even a meaningful contributor to  
 173 ET's variability. To better understand  $D$ 's contribution, we normalize  $\frac{\partial ET}{\partial D}$  with  $D$ 's standard  
 174 deviation to define a (linearized) relative change in ET for variations in  $D$ .  $D$ 's contribu-  
 175 tion to ET's variability ranges between 16 - 20 W m<sup>-2</sup> for all PFTs except for CSH, which  
 176 is about 51 W m<sup>-2</sup>. Another meaningful comparison is to  $\frac{\partial ET}{\partial R} * std(R)$ , as net radiation is  
 177 generally the driver of ET (cite joe berry here). For all PFTs except for CSH  $D$  contributes  
 178 between 14.5 - 20.5 % of  $R$ 's contribution to variability. For CSH the portion is much larger,  
 179 about 44 %.  $D$ 's variability is certainly a non-negligible contributor to ET's variability.

180 So far, idealized plots and statistics have illuminated the form of  $\frac{\partial ET}{\partial D}$  and how it varies  
 181 with PFT. Large mean  $\sigma$  and uWUE shifts CRO and DBF towards positive  $\frac{\partial ET}{\partial D}$ . However,  
 182 the strongly nonlinear function of  $\frac{\partial ET}{\partial D}$  at  $\frac{\partial ET}{\partial D} < 0$  pushes  $\frac{\partial ET}{\partial D}$  negative for DBF (it does  
 183 not do this for CRO because of CRO's high  $g_1$ ). ENF's low  $g_1$  value increases the depen-  
 184 dence of  $\frac{\partial ET}{\partial D}$  on  $D$ , and makes the function more strongly nonlinear. This has the side effect

193

**Table 3.** Statistics of  $\frac{\partial ET}{\partial D}$  as a function of PFT.

PFT	$\frac{\partial ET}{\partial VPD}$	$\overline{\frac{\partial ET}{\partial D}(T, \dots, D)}$	$\overline{\frac{\partial ET}{\partial D}(T, \dots, D)} * \text{std}(D)$	$\frac{\partial ET}{\partial D}(\overline{T, \dots, D}) * \text{std}(D)$	fraction $\frac{\partial ET}{\partial VPD} < 0$
CRO	0.000853	0.026241	18.523659	0.203022	0.473311
CSH	-0.108234	-0.091526	50.861613	0.439379	0.931660
DBF	-0.012727	0.013794	19.734435	0.164241	0.461674
ENF	-0.034087	0.000706	16.611852	0.148548	0.534425
GRA	-0.019637	-0.000921	16.798083	0.173552	0.631735

<sup>a</sup>Footnote text here.

185 of pushing  $\overline{\frac{\partial ET}{\partial D}}$  negative further than other PFTs for a given fraction  $\frac{\partial ET}{\partial D} < 0$  and magni-  
 186 tude  $\overline{\frac{\partial ET}{\partial D}(T, \dots, D)}$ . GRA shows the opposite behavior; a relatively high  $g_1$  makes the func-  
 187 tion more linear, decreasing the magnitude of  $-\overline{\frac{\partial ET}{\partial D}}$  for a given [large] fraction  $\frac{\partial ET}{\partial D} < 0$   
 188 and negative  $\overline{\frac{\partial ET}{\partial D}(T, \dots, D)}$  (although  $g_a$  and Term 1 also probably have a role in this). Fi-  
 189 nally, low  $uWUE$  of CSH pushes toward by far the lowest values  $\frac{\partial ET}{\partial D}$  (Figure 5). Vari-  
 190 ability in  $D$  accounts for the largest about of  $ET$  variability for CSH. For the other PFTs,  $D$   
 191 contributes less to  $ET$  variability, but still represents about 15-20 % of  $R$ 's contributions to  
 192  $ET$  variability.

#### 194 4.1 Full observations of $\frac{\partial ET}{\partial D}$

195 Now that we have an intuitive understanding of  $\frac{\partial ET}{\partial D}$ 's behavior, we are equipped to  
 196 interpret fully realistic plots of  $\frac{\partial ET}{\partial D}$  for each PFT. Figure 6 presents calculated  $\frac{\partial ET}{\partial D}$  where,  
 197 unless otherwise noted, all variables in Equation 7 are allowed to vary. Each column is a  
 198 different quantity related to  $\frac{\partial ET}{\partial D}$ , and each row is a different PFT.

199 The full observations generally confirm expectations from Section 4. CRO has the  
 200 most positive values of  $\frac{\partial ET}{\partial D}$ ,  $\frac{\partial ET}{\partial D}$  is almost always negative for CSH, and response depends  
 201 more with the environmental conditions for the other PFTs (especially ENF). Through the  
 202 columns of Figure 6 we can see the impact of  $\sigma$  and  $g_a$  on the variability of  $\frac{\partial ET}{\partial D}$ .  $g_a$ 's scal-  
 203 ing (included in columns 1 and 3) alters the magnitude considerably.  $\sigma$  variability (included  
 204 in columns 1 and 2) adds a lot of additional noise to the signal of  $\frac{\partial ET}{\partial D}$ , which is slightly un-  
 205 desirable given  $\sigma$ 's role in representing model and observational uncertainty. However, the  
 206 general story with the noise appears to match the cleaner signal when  $\sigma$  is help constant and

207  $D_{ETmin}$  is clearly visible . One exception is possibly with GRA, for which uncertainty repre-  
 208 sented in  $\sigma$  is high and causes the full complexity plots (Columns 1 and 2) to not match well  
 209 with  $\sigma$  held fixed (Columns 3 and 4).

← I really need  
to make  
these plots  
better - way  
too much  
overlapping  
of points  
that hurts the  
story

210 For ENF and GRA  $D_{ETmin}$  does not appear to be only a function of  $\sigma$  (most observ-  
 211 able in Column 4). It turns out that the site to site variability in  $\gamma$  causes  $D_{ETmin}$  to vary,  
 212 which is not discussed in the previous section. The impact is observable in both ENF and  
 213 GRA, but especially for ENF which has a larger  $\frac{\partial^2 ET}{\partial^2 D}$  than the other PFTs.

214 In general the full complexity plots of  $\frac{\partial ET}{\partial D}$  match our expectations, even with the large  
 215 sensitivity to  $\sigma$  measures of uncertainty observed in Figure 5. Our  $\sigma$ -based method of un-  
 216 certainty propagation blurs the idealized expectations the most for GRA, and also has a con-  
 217 siderable effect for CRO. We therefor have the most confidence in our conclusion based on  
 218 Equation 7 for PFTS CSH, DBF, and ENF, as the full complexity plots with uncertainty in-  
 219 cluded closely match the story when  $\sigma$  is held fixed. \*\*see somewhat preferred alternate  
 220 figure 7 .

← I think I like  
the alternate  
plot much  
more as  
thinking in  
terms of T  
and RH is  
easier, and  
it makes the  
story easier  
to see at rel-  
atively low  
temperatures.  
However,  
I used the  
other plot be-  
cause Fig 5  
does not dis-  
cuss things  
in terms of  
temperature,  
as this would  
make things  
more compli-  
cated (adding  
another di-  
mension).  
I could just  
include both  
versions  
of figure 6  
though (us-  
ing figure 6a  
as a bridge to  
figure 6b)

## 221 5 Conclusions

222 The idealized representation of ET used here is successful in developing intuition for  
 223 how ET responds to changes in  $D$ . This intuition will aid the community in interpreting ob-  
 224 servations and output from sophisticated full complexity climate models.

225 The idealized framework leads to the following general conclusions:

- 226 • Aerodynamic resistance plays an important role of scaling  $\frac{\partial ET}{\partial D}$ . This is a leading  
 227 order effect for observing higher magnitude responses in DBF and ENF.
- 228 • In general, CSH has the most negative (i.e. ET reduced) response to increases in  $D$   
 229 (atmospheric drying). So CSH plants will almost always try and conserve water, ef-  
 230 fectively reducing ET with dry atmospheric perturbation.
- 231 • Additionally for CSH,  $D$  variability contributes the most to  $ET$  variability.
- 232 • CRO has the most positive response (i.e. ET increased) in response to increases in  
 233  $D$ . This is consistent with CROs that may be evolved or bred to thrive in non-water-  
 234 limited environments.
- 235 • The response is more a function of the environment for DBF, ENF, and GRA. Be-  
 236 cause as VPD increases the response is more likely to be positive, if RH is fixed then

← also need  
to flesh this  
section out

245 the response will be more likely to be positive at warmer T, or if T is fixed the re-  
 246 sponse is more likely to be positive with decreasing RH.

- 247 • ENF has the strongest dependence on environmental conditions due to its small  $g_1$ .
- 248 • Model and observational uncertainty is highest for GRA and CRO, so conclusions  
 249 about those PFTs should be tempered.
- 250 • However, inclusion of uncertainty doesn't alter conclusions about DBF, ENF, and  
 251 CSH.

252 The intuition developed using this framework can be used to understand how the land  
 253 surface will respond and contribute to changes in the environment.

#### 254 **Acknowledgments**

255 This work used eddy covariance data acquired and shared by the FLUXNET community, in-  
 256 cluding these networks: AmeriFlux, AfriFlux, AsiaFlux, CarboAfrica, CarboEuropeIP, Car-  
 257 boItaly, CarboMont, ChinaFlux, Fluxnet-Canada, GreenGrass, ICOS, KoFlux, LBA, NECC,  
 258 OzFlux-TERN, TCOS-Siberia, and USCCC. The ERA-Interim reanalysis data are provided  
 259 by ECMWF and processed by LSCE. The FLUXNET eddy covariance data processing and  
 260 harmonization was carried out by the European Fluxes Database Cluster, AmeriFlux Man-  
 261 agement Project, and Fluxdata project of FLUXNET, with the support of CDIAC and ICOS  
 262 Ecosystem Thematic Center, and the OzFlux, ChinaFlux and AsiaFlux offices.

#### 263 **References**

- 264 Ball, J. T., I. E. Woodrow, and J. A. Berry (1987), A model predicting stomatal conductance  
 265 and its contribution to the control of photosynthesis under different environmental con-  
 266 ditions, in *Progress in Photosynthesis Research*, pp. 221–224, Springer Netherlands, doi:  
 267 10.1007/978-94-017-0519-6\_48.
- 268 Franks, P. J., J. A. Berry, D. L. Lombardozzi, and G. B. Bonan (2017), Stomatal function  
 269 across temporal and spatial scales: Deep-time trends, land-atmosphere coupling and  
 270 global models, *Plant Physiology*, 174(2), 583–602, doi:10.1104/pp.17.00287.
- 271 Leuning, R. (1990), Modelling stomatal behaviour and and photosynthesis ofEucalyptus  
 272 grandis, *Australian Journal of Plant Physiology*, 17(2), 159, doi:10.1071/pp9900159.
- 273 Lin, Y.-S., B. E. Medlyn, R. A. Duursma, I. C. Prentice, H. Wang, S. Baig, D. Eamus, V. R.  
 274 de Dios, P. Mitchell, D. S. Ellsworth, M. O. de Beeck, G. Wallin, J. Uddling, L. Tarvainen,

275 M.-L. Linderson, L. A. Cernusak, J. B. Nippert, T. W. Ocheltree, D. T. Tissue, N. K.  
 276 Martin-StPaul, A. Rogers, J. M. Warren, P. D. Angelis, K. Hikosaka, Q. Han, Y. Onoda,  
 277 T. E. Gimeno, C. V. M. Barton, J. Bennie, D. Bonal, A. Bosc, M. LÃºw, C. Macinins-  
 278 Ng, A. Rey, L. Rowland, S. A. Setterfield, S. Tausz-Posch, J. Zaragoza-Castells, M. S. J.  
 279 Broadmeadow, J. E. Drake, M. Freeman, O. Ghannoum, L. B. Hutley, J. W. Kelly,  
 280 K. Kikuzawa, P. Kolari, K. Koyama, J.-M. Limousin, P. Meir, A. C. L. da Costa, T. N.  
 281 Mikkelsen, N. Salinas, W. Sun, and L. Wingate (2015), Optimal stomatal behaviour  
 282 around the world, *Nature Climate Change*, 5(5), 459–464, doi:10.1038/nclimate2550.

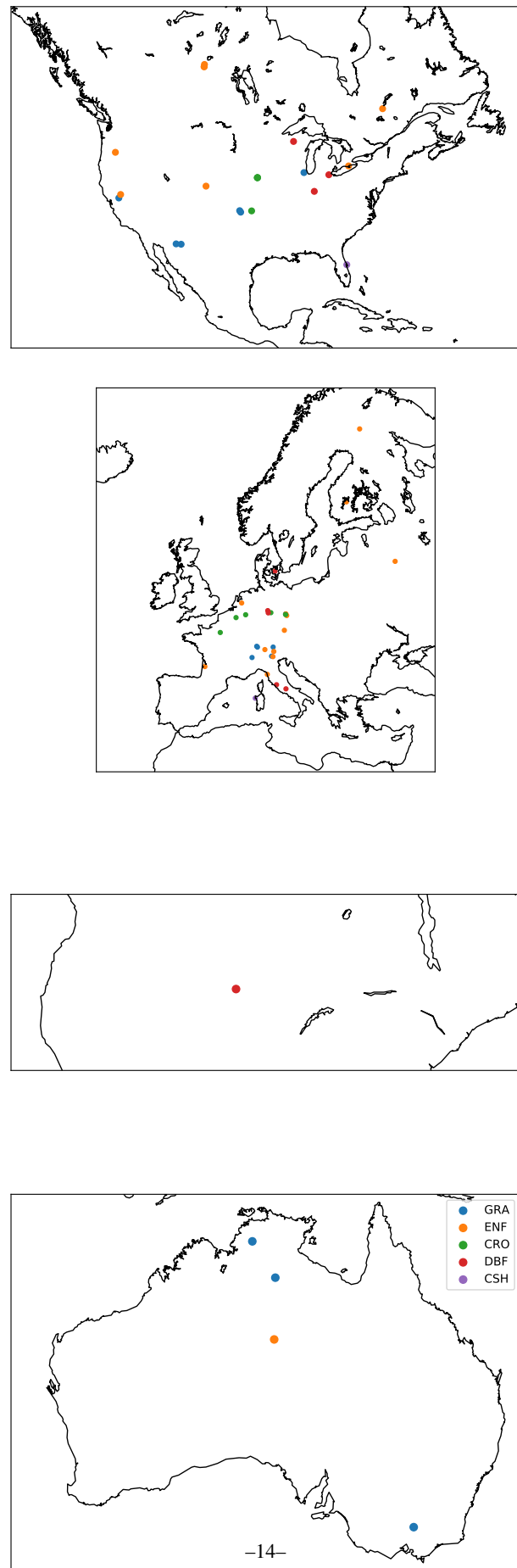
283 MEDLYN, B. E., R. A. DUURSMA, D. EAMUS, D. S. ELLSWORTH, I. C. PRENTICE,  
 284 C. V. M. BARTON, K. Y. CROUS, P. D. ANGELIS, M. FREEMAN, and L. WINGATE  
 285 (2011), Reconciling the optimal and empirical approaches to modelling stomatal conduc-  
 286 tance, *Global Change Biology*, 17(6), 2134–2144, doi:10.1111/j.1365-2486.2010.02375.x.

287 Zhou, S., B. Yu, Y. Huang, and G. Wang (2015), Daily underlying water use efficiency for  
 288 AmeriFlux sites, *Journal of Geophysical Research: Biogeosciences*, 120(5), 887–902, doi:  
 289 10.1002/2015jg002947.

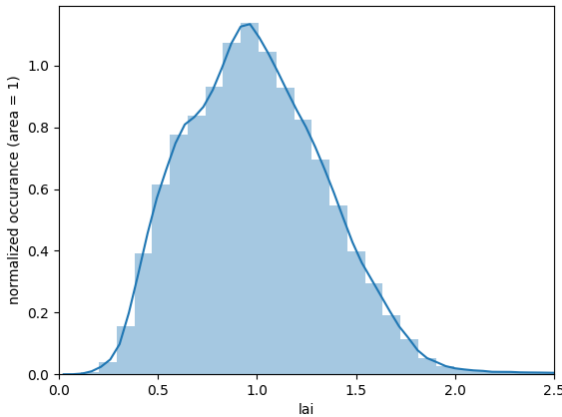
## 290 References

- 291 Ball, J. T., I. E. Woodrow, and J. A. Berry (1987), A model predicting stomatal conductance  
 292 and its contribution to the control of photosynthesis under different environmental con-  
 293 ditions, in *Progress in Photosynthesis Research*, pp. 221–224, Springer Netherlands, doi:  
 294 10.1007/978-94-017-0519-6\_48.
- 295 Franks, P. J., J. A. Berry, D. L. Lombardozzi, and G. B. Bonan (2017), Stomatal function  
 296 across temporal and spatial scales: Deep-time trends, land-atmosphere coupling and  
 297 global models, *Plant Physiology*, 174(2), 583–602, doi:10.1104/pp.17.00287.
- 298 Leuning, R. (1990), Modelling stomatal behaviour and and photosynthesis ofEucalyptus  
 299 grandis, *Australian Journal of Plant Physiology*, 17(2), 159, doi:10.1071/pp9900159.
- 300 Lin, Y.-S., B. E. Medlyn, R. A. Duursma, I. C. Prentice, H. Wang, S. Baig, D. Eamus, V. R.  
 301 de Dios, P. Mitchell, D. S. Ellsworth, M. O. de Beeck, G. Wallin, J. Uddling, L. Tarvainen,  
 302 M.-L. Linderson, L. A. Cernusak, J. B. Nippert, T. W. Ocheltree, D. T. Tissue, N. K.  
 303 Martin-StPaul, A. Rogers, J. M. Warren, P. D. Angelis, K. Hikosaka, Q. Han, Y. Onoda,  
 304 T. E. Gimeno, C. V. M. Barton, J. Bennie, D. Bonal, A. Bosc, M. LÃºw, C. Macinins-  
 305 Ng, A. Rey, L. Rowland, S. A. Setterfield, S. Tausz-Posch, J. Zaragoza-Castells, M. S. J.  
 306 Broadmeadow, J. E. Drake, M. Freeman, O. Ghannoum, L. B. Hutley, J. W. Kelly,

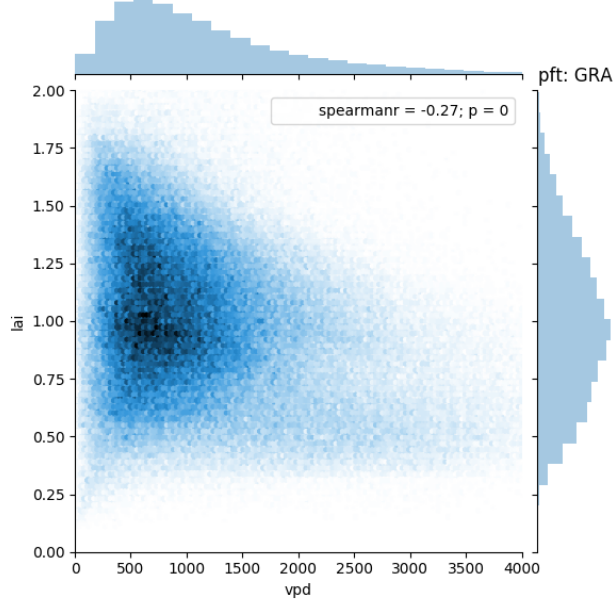
- 307 K. Kikuzawa, P. Kolari, K. Koyama, J.-M. Limousin, P. Meir, A. C. L. da Costa, T. N.  
308 Mikkelsen, N. Salinas, W. Sun, and L. Wingate (2015), Optimal stomatal behaviour  
309 around the world, *Nature Climate Change*, 5(5), 459–464, doi:10.1038/nclimate2550.
- 310 MEDLYN, B. E., R. A. DUURSMA, D. EAMUS, D. S. ELLSWORTH, I. C. PRENTICE,  
311 C. V. M. BARTON, K. Y. CROUS, P. D. ANGELIS, M. FREEMAN, and L. WINGATE  
312 (2011), Reconciling the optimal and empirical approaches to modelling stomatal conduc-  
313 tance, *Global Change Biology*, 17(6), 2134–2144, doi:10.1111/j.1365-2486.2010.02375.x.
- 314 Zhou, S., B. Yu, Y. Huang, and G. Wang (2015), Daily underlying water use efficiency for  
315 AmeriFlux sites, *Journal of Geophysical Research: Biogeosciences*, 120(5), 887–902, doi:  
316 10.1002/2015jg002947.



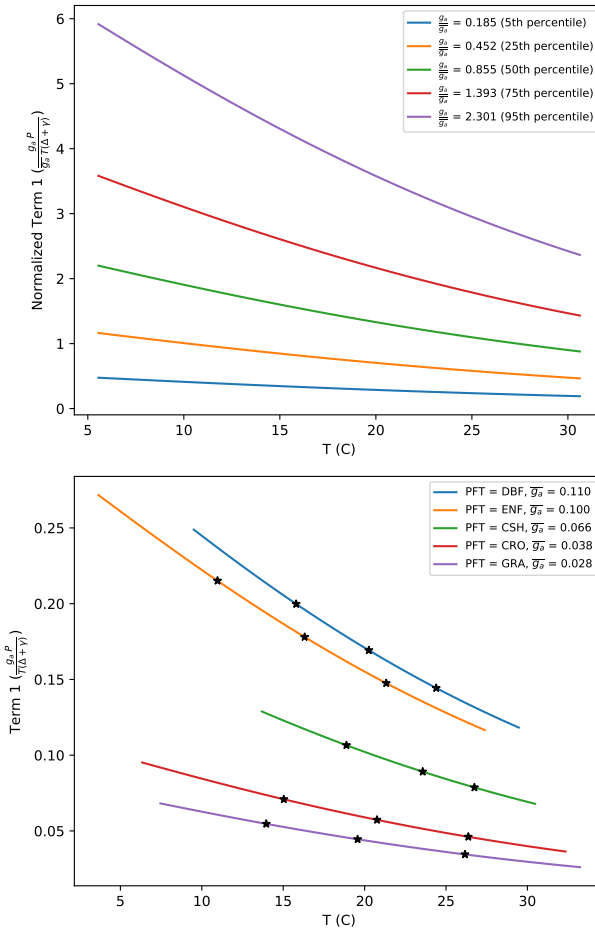
90 **Figure 1.** Plant functional type and location of sites used in analysis. \*\*\*This is just a placeholder for now  
91 and needs to be improved i.e. with lat lon, better placement of continents, etc.)\*\*\*



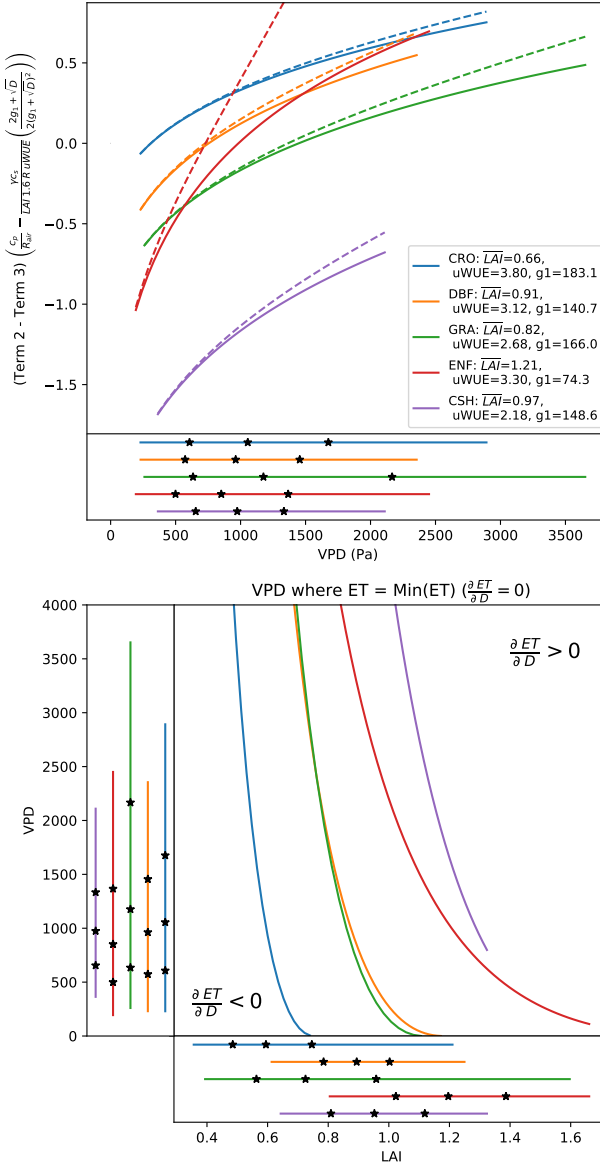
103 **Figure 2.** Histogram of  $\sigma$  values calculated for each site and time according to Equation 9.  
 104 The lowest and highest 5% are removed as outliers, as well as any values below 0.  
 105 The curve is normalized such that its area is 1.



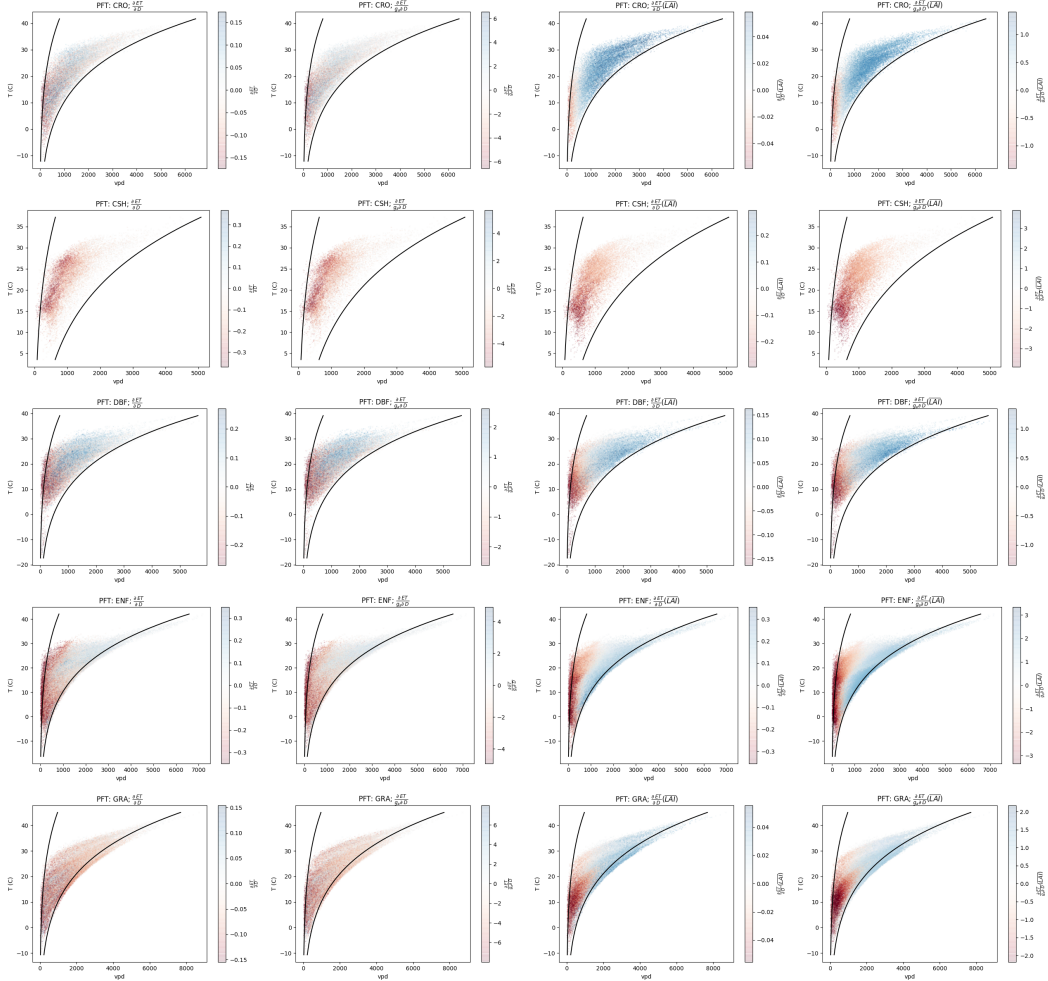
111 **Figure 3.** The joint distribution of  $D$  and  $\sigma$ .  $\sigma$  has only a weak dependence on  $D$ . \*\*\*This plot could  
 112 probably benefit from a box plot of site specific correlations, because some sites do have stronger depen-  
 113 dence than others. Note also Figs 3 and 2 can probably be combined because this figure shows  $\sigma$ 's his-  
 114 togram.\*\*\*



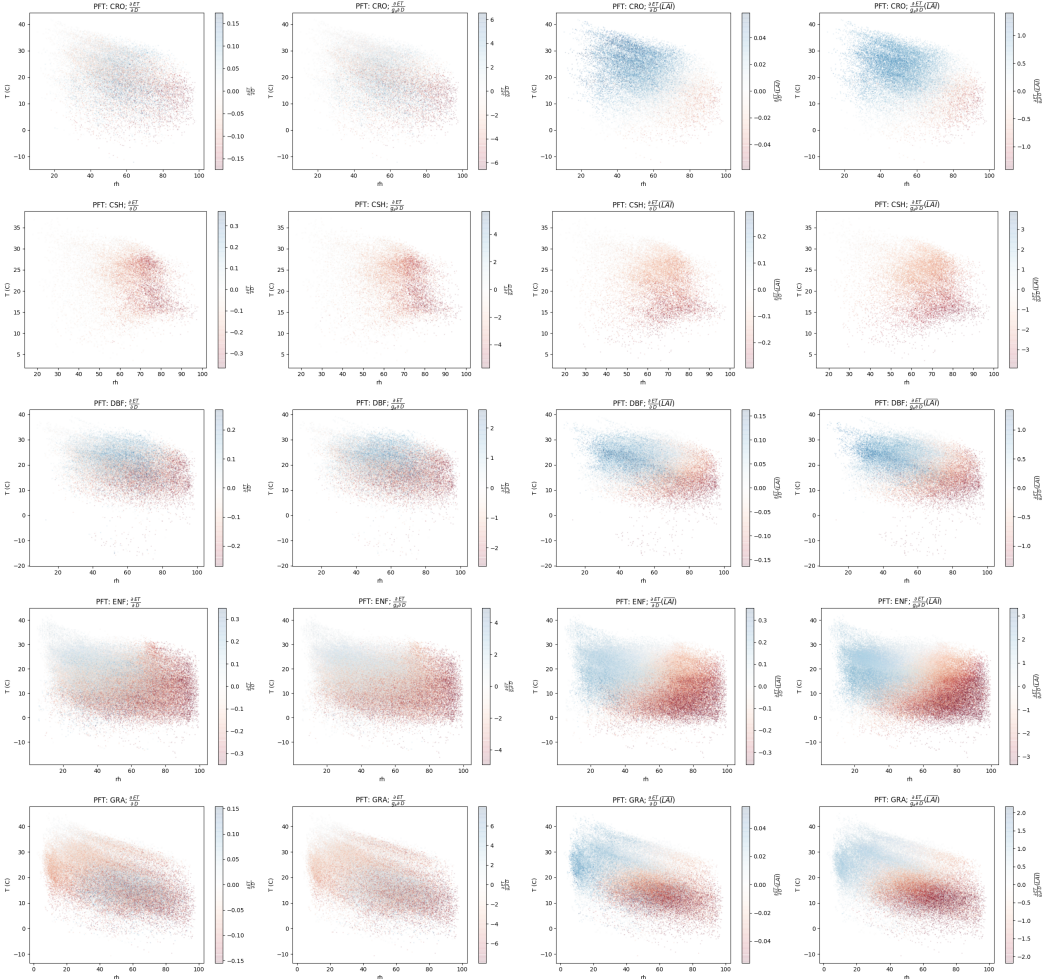
143 **Figure 4.** Primary sources of variability for Term 1. A) Variability within each PFT: Term 1 normalized by  
 144 mean  $g_a$  for each PFT. B) Variability between each PFT: Term 1 evaluated at mean  $g_a$  for each PFT. Tempera-  
 145 ture range is 5-95th percentile for each PFT. Additionally, stars denote the location of the 25th, 50th, and 75th  
 146 percentiles.



154 **Figure 5.** Sources of variability for Term 2 - Term 3. Top: Term 2 - Term 3 as a function of VPD, with  $\sigma$   
 155 held fixed at PFT averages. The observed range of VPD for each PFT is also shown below the x-axis. Line  
 156 extent corresponds to 5th and 95th percentiles, while stars denote the location of the 25th, 50th, and 75th  
 157 percentiles.  
 158 Bottom: The location of the minima of ET, as a function of VPD and  $\sigma$ . Lines and stars denote the distribu-  
 159 tion of VPD and  $\sigma$  next to each axis, following the same percentiles as above.



214 **Figure 6.** Scatter plots of  $\frac{\partial ET}{\partial D}$ . Each row is a different PFT, and each column is a different quantity related  
 215 to  $\frac{\partial ET}{\partial D}$ , as labeled: Column 1 -  $\frac{\partial ET}{\partial D}$ ; Column 2 -  $\frac{\partial ET}{\partial D}$  normalized by  $g_a$ ; Column 3 -  $\frac{\partial ET}{\partial D}$  with  $\sigma$  held  
 216 fixed at PFT average; and Column 4 -  $\frac{\partial ET}{\partial D}$  normalized by  $g_a$  and with  $\sigma$  held fixed. For reference, lines  
 217 corresponding to RH = 20% and RH = 90 % are drawn. Please note differences in the colorbar scale. \*\*\*see  
 218 alternate (or additional) plot below.\*\*\*



226 **Figure 7.** \*\*\*\*alternate Fig 06\*\*\*\* Scatter plots of  $\frac{\partial ET}{\partial D}$ . Each row is a different PFT, and each column  
 227 is a different quantity related to  $\frac{\partial ET}{\partial D}$ , as labeled. If I end up using this, I could also draw on the curve of  
 228  $D_{ETmin}$  with  $\overline{LAI}_{ref}$ .